SUPPORTING INFORMATION

Rapid binding and release of Hfq from ternary complexes during RNA annealing

Julia F. Hopkins, Subrata Panja, and Sarah A. Woodson

Johns Hopkins University, 3400 N. Charles St., Baltimore, MD 21218, USA

FIGURE S1

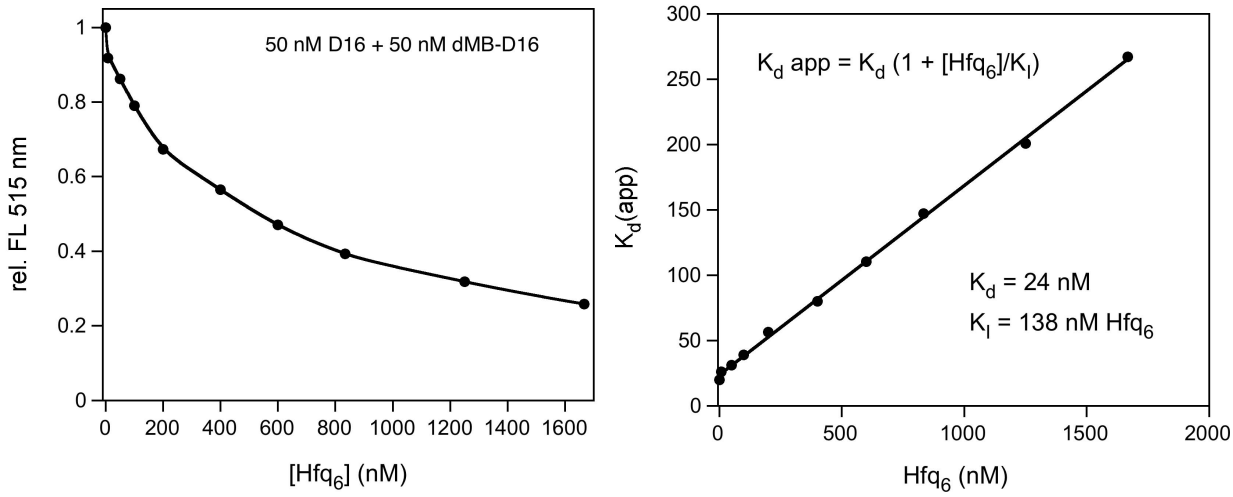

Figure S1. Effect of Hfq on equilibrium endpoint of RNA-beacon annealing. Left, 50 nM D16 RNA and 50 nM dMB-D16 beacon were allowed to base pair, and the relative fluorescence intensity of the RNA-beacon duplex measured at 515 nM at equilibrium. Hfq protein was added and samples equilibrated after each addition before the fluorescence was recorded. Right, the concentration of RNA-beacon duplex (DB) and apparent dissociation constant for the duplex were calculated from the change in fluorescence. Plot of K_d(app) vs. [Hfq_6] is consistent with competitive inhibition model. The K_d obtained from this titration was close to that measured from direct tirations (24 vs 19.6 nM); the K_I for Hfq is greater than expected based on association of Hfq with single-stranded D16 (138 vs. 23 nM).

FIGURE S2

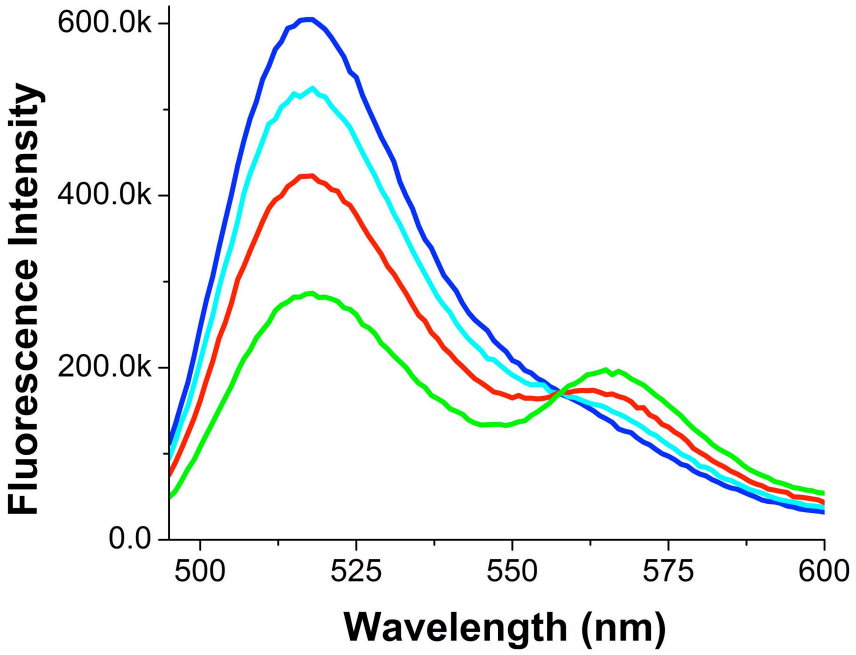

Figure S2. FRET assay for Hfq-RNA binding. Fluorescence emission of Hfq-Cy3 and D16-FL RNA complexes, with excitation at 495 nm (Horiba Fluoromax 1.1). D16-FAM (100 nM) was titrated with Hfq-Cy3 in TNK buffer at 30^0C, resulting in lower emission at 515 nM (FAM donor) and higher emission at 565 nm (Cy3 acceptor). Hfq monomer concentrations were 0 nM (blue), 248 nM (cyan), 496 nM (red), 1240 nM (green). For stopped-flow experiments, the decrease in FAM emission at 515 nm was measured using a 520 (±10) nm band pass filter.

FIGURE S3

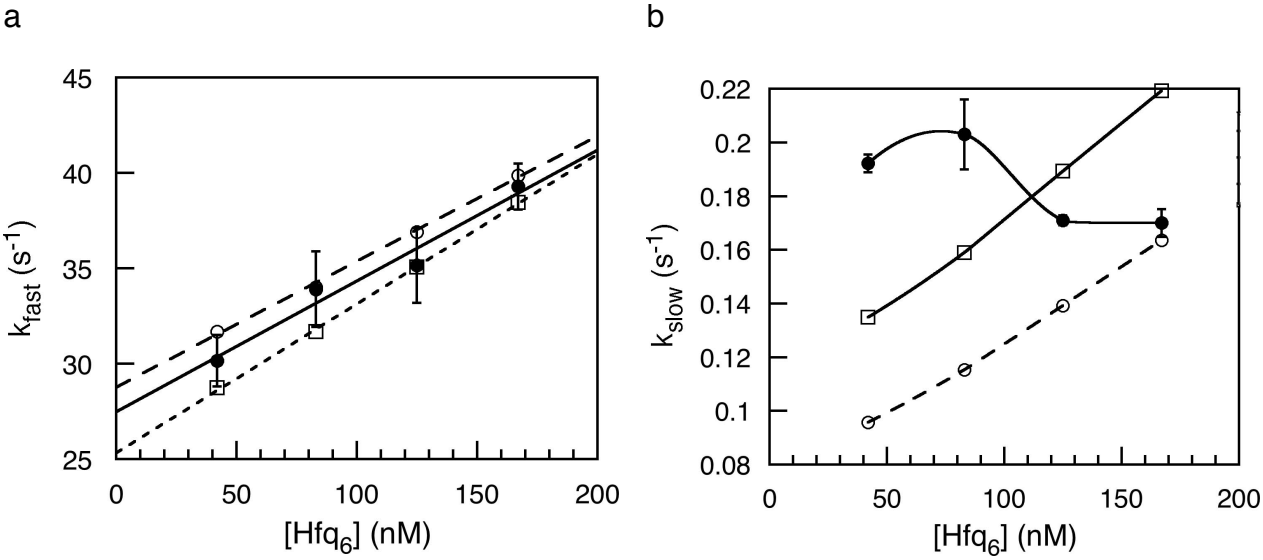

Figure S3. Hfq-RNA binding kinetics. Experimental progress curves for binding of 50 nM D16-FL with Hfq-Cy3 were simulated with the mechanism in Scheme I (Berkeley Madonna). (a) Comparison of parameters for fast binding step. Filled circles, experimental values from the linear fit are; k_{on} (k1f) = 6.9 • 10^7 $M^{-1}s^{-1}$, k1r = 27 s^{-1}. Open squares, simulation 1: k1f = 8.5 • 10^7 $M^{-1}s^{-1}$, k1r = 23 s^{-1}, k2f = 0.5 s^{-1}, k2r = 0.05 s^{-1}; open squares, simulation 2: k1f = 7.0 • 10^7 $M^{-1}s^{-1}$, k1r = 27 s^{-1}, k2f = 0.5 s^{-1}, k2r = 0.03 s^{-1}. (b) Parameters for slow step. Symbols and simulation parameters as in a.

FIGURE S4

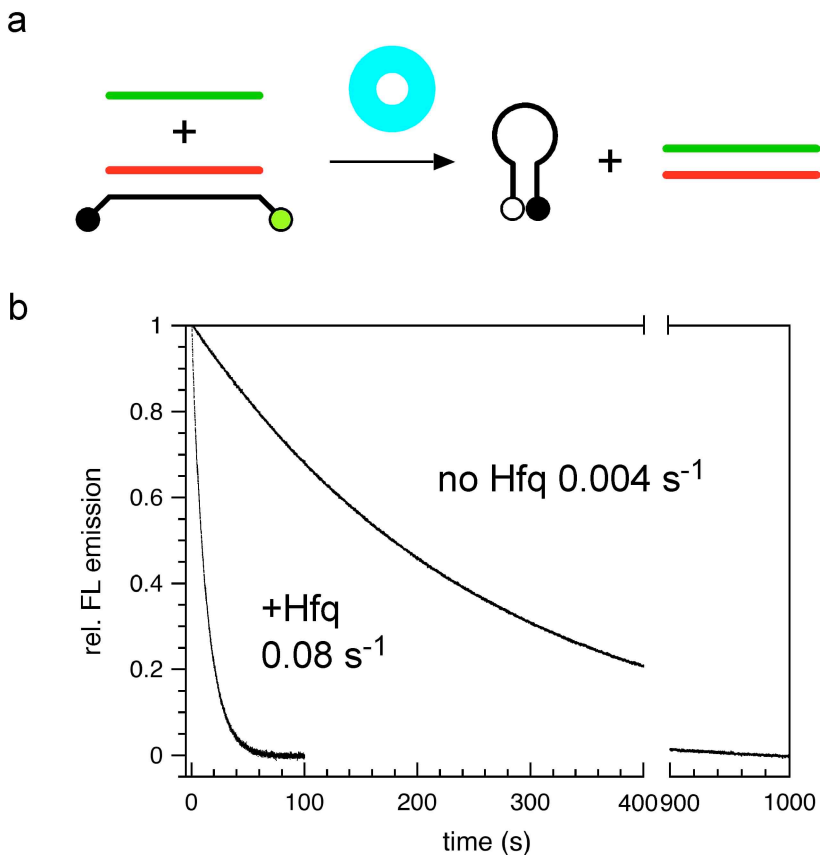

Figure S4. Hfq accelerates strand exchange. (a) Rate of strand exchange measured by challenging 50 nM dMB-D16 • D16 RNA complex with 50 nM R16 RNA. (b) Release of the beacon upon exchange with R16 RNA decreases the fluorescence emission. Observed rates were 0.004 s^{-1} in the absence of Hfq and 0.08 s^{-1} with 50 nM Hfq_6. Similar results were obtained if Hfq was added to the syringe containing R16 RNA or dMB-D16 • D16 RNA. The strand exchange kinetics is consistent with earlier results in 200 nM Hfq_6 (25).

FIGURE S5

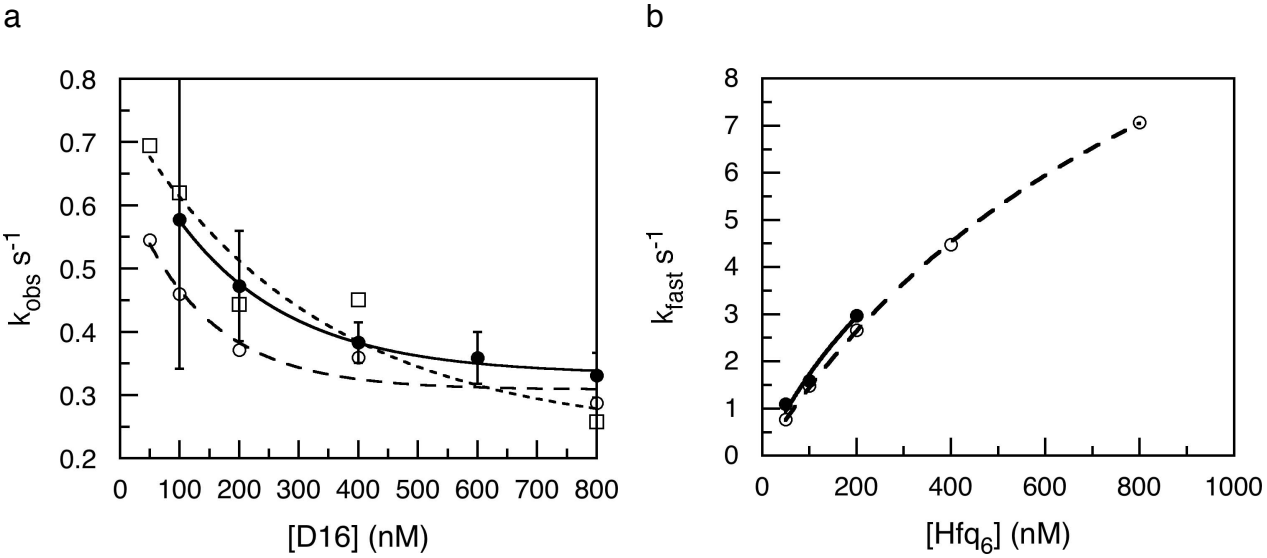

Figure S5. Simulations of Hfq-dependent RNA annealing kinetics. Annealing of 50 nM dMB-D16 and D16 RNA in TNK buffer was simulated using the mechanism in Fig. 6. (a) Dependence on D16 RNA, in 50 nM Hfq_6. Filled circles, experimental data (see Fig. 5); open circles, simulation 1; open squares, simulation 2. (b) Hfq dependence, with 100 nM D16. Rate constants for DH binding were k1f = $7.0 \bullet 10^7$ $M^{-1}s^{-1}$, k1r = 27 s^{-1}, k2f = 0.5 s^{-1}, k2r = 0.05 s^{-1} (DHs was assumed to be inert). Rate constants for forming the DHD complex were k3f = $7.0 \bullet 10^7$ $M^{-1}s^{-1}$, k3r = 5.7 s^{-1}, and forming the ternary complex and Hfq release were k4f = $1.0 \bullet 10^8$ $M^{-1}s^{-1}$, k4r = 16 s^{-1}, k5f = 20 s^{-1}, k5r = $1.0 \bullet 10^7$ $M^{-1}s^{-1}$. Final steps of helix zippering or strand dissociation were assumed to be fast. Simulations included the Hfq-independent pathway for annealing, $k_{on} = 3.4 \bullet 10^4$ $M^{-1}s^{-1}$; $k_{off} = 6.7 \bullet 10^{-4}$ s^{-1}. Parameters for simulation 2 were as above, except k3r = 5.0 s^{-1}; k4f = $1.5 \bullet 10^8$ $M^{-1}s^{-1}$, k4r = 22 s^{-1}.